The

ALFOSC Camera

Pre-commissioning characterisation of CCD and cryostat

Anton Norup Sørensen
Copenhagen University Observatory

February 1998

Contents

1 Introduction 2

2 Operating options 2

3 Cosmetics 2

4 Read-out noise 3

5 Cross-talk 3

6 Gain, linearity and full-well 3

7 Charge Transfer Efficiency 4

8 Modulation Transfer Function 4

9 Quantum-efficiency 5

10 Bias and overscan 6

11 Dark current 7

12 Pixel size 7

13 Cryostat 8

1 Introduction

This document describes the performance of the W19-(0,0) CCD, installed in a cryostat specifically for the ALFOSC, as measured in the laboratory of Copenhagen University Observatory. The CCD was tested using the controller that will also be used when the camera is commissioned on the ALFOSC, so the test results are expected to be very close to what is found under observing conditions.

The CCD is a Ford-Loral three side buttable with 2048^2 imaging pixels, each $15\mu m$ square. Packaging for back-side illumination, "ultra-thinning" and coating was performed by the Steward Observatory CCD Laboratory. The CCD is anti-reflection coated using HfO_2 for maximum QE around 475nm, and for high blue QE it has a "Cat-C" coating that has proved practically maintenance-free. The CCD is intended to replace the previous ALFOSC CCD, that required UV-flooding for good blue QE, but did not deliver stable sensitivity. All tests at CUO indicate that this problem will be eliminated with the new CCD.

2 Operating options

The CCD has two functional output amplifiers, 'A' and 'B'. These can be selected individually or used simultaneously. Default is 'B' only. Before using both amplifiers simultaneously, one should consider the consequences of cross-talk and a more complicated reduction due to different gain and bias behavior.

The parallel phases can be operated in "normal" or "mpp" mode. Default is mpp, where dark current is minimized. Slightly better spatial resolution is achieved by selecting normal mode, but at the cost of higher dark current.

Operating temperature is normally -100°C, and testing has only been performed at this temperature.

Two ADU conversion factors can be selected, "high" or "low". "high" gain is default and offers the best signal to noise ratio at the expense of a slightly reduced dynamic range.

The area to be read out may be specified by any rectangular section, and on-chip pixel binning may be specified independently in the x and y directions.

In addition to four columns of physical overscan, a larger overscan region can be generated by continued clocking. Size is programmable, with a default of 50 columns, but it is required that the read-out window extends to one edge of the CCD.

3 Cosmetics

Flat fields at different wavelengths are shown in figures 6, 7 and 8.

The large scale uniformity is very good in the middle of the optical band, with variation of about 1% over the field. As the CCD is nearly transparent at the longest detectable wavelengths, thickness variations and internal reflections makes the non-uniformities increase to typically 5%, with a single deviation of up to 20%. In the near-UV, a 5% diagonal gradient in sensitivity is seen. At the extreme corners and edges, sensitivity goes down as the chip is not thinned there.

Specks a few pixels wide having reduced sensitivity are scattered over the entire imaging area. Setting a threshold 5% lower than the median sensitivity, 1% of the area is affected by the specks. The central sensitivity in the specks typically goes down by 20%, but a few areas goes much lower. All of the specks can be corrected by flat-fielding. There appears to at least two types of specks. Some are probably an opaque deposit on the surface, like the scratch and dust-like structures, others are probably defects in the coating - more on these later.

Charge traps and bad columns can be found by comparing a flat field exposure at very low illumination level to a well exposed one, as illustrated in figure 1. In the table below, the coordinates of defects found are listed. Note that the number of pixels affected by a trap depends on the illumination level. The actual trap location is the smallest Y-coordinate of the area.

Low level traps	Comment
$[64, 605 : 618]$	
$[585, 123 : 142]$	
$[587, 1027 : 1030]$	
$[685, 1210 : 1213]$	
$[1029, 274 : 278]$	
$[1251, 1789 : 1791]$	
$[1300, 870 : 886]$	
$[1458, 732 : 762]$	
$[1728, 361 : 525]$	
$[1762, 304 : 331]$	
High level traps or bad columns	
$[1281, 255 : 2048]$	Skimming or bad CTE in column above trap.
$[2002, 1471 : 2048]$	Not seen a low light level. Skimming or bad CTE above.
$[2024, 720 : 2048]$	Deep trap. Skimming or bad CTE in column above trap.
$[623, 2008 : 2048]$	Bad column
$[1041 : 1042, 1255 : 2048]$	Bad columns
$[1835 : 1836, 1388 : 2048]$	Bad columns
Other	
$[1409 : 1426, 460 : 476]$	Largest spot with low QE, less than 10% of surroundings

If the CCD is warmer than -90°C, a group of about 10 warm columns will appear around column x=216.

4 Read-out noise

Noise measured in bias frames with 1*1 binning, mpp+ mode:

	Amplifier A	Amplifier B
High gain:	6.7 e^-	5.6 e^-
Low gain:	8.2 e^-	7.8 e^-

Measurements of RON in amplifier B using 2 by 2 binning gave values identical to the 1 by 1 binning RON. Reading out using higher binning may induce a pattern of a few ADU in amplitude, effectively increasing read out noise.

5 Cross-talk

In dual read-out mode, cross-talk occurs between the two amplifiers. An image of a star in one side of the image will then have a fainter electronic ghost image mirrored around the border of the two image sections. Measurements on CCD cameras of the same type as the one tested here resulted in a crosstalk strength of the order 10^{-4}. This means that the ghost image of a bright source will easily be detected, and one should consider carefully whether dual readout is compatible with the planned observations.

6 Gain, linearity and full-well

Gain measured from Poisson noise statistics shows a strong dependency on the exposure level on some CUO cameras. For the W19-(0,0) , the relation found is plotted in figure 2, indicating a deviation from linearity of about 5%.

A more precise measurement of linearity is reached by measuring the ADU level versus exposure time, using a stable light source. Measurements made in this way are plotted in figure 3. By dividing the counts with the exposure time, corrected for shutter delay, no significant linearity deviation is found from 10ADU to 63000ADU in the high gain range of amplifier B. There is a considerable scatter in the data, making the smallest detectable linearity deviation about 0.5%. A more careful tracking of the lamp intensity is expected to reduce the scatter.

The Poisson noise analysis clearly is wrong. A noise modulation/source must be causing this, but the origin is currently unknown.

From analysis of photon noise statistics and Fe-55 impacts, the following conversion factors were found:

	Amplifier A	Amplifier B
High gain, Poisson:	1.05 e^-/ADU	1.02 e^-/ADU
High gain, Fe-55:	1.13 e^-/ADU	1.09 e^-/ADU
Low gain, Poisson:	3.00 e^-/ADU	2.92 e^-/ADU

Note that there is a discrepany between the Poisson and Fe-55 gain. In this text, the Poisson-derived gain is used for ADU to electron conversion.

At an illumination level of 101.000e-, saturation is evident as a decrease in noise in a flat field image, while at 90.000e-, no saturation effects are seen using either amplifier. As the high-gain is approx. 1.0 e^-/ADU, the entire high-gain dynamic range is below saturation. A low-gain of about 3 e^-/ADU places the saturation level in the middle of the low-gain ADU range, making low-gain mode not very useful.

Listed below is the highest illumination level where saturation effects have not been seen. ADU count is for low-gain.

	Amplifier A	Amplifier B
MPP+ 1*1 bins	102000 e^- / 34000 ADU	90000 e^- / 31000 ADU

In MPP– mode, full well is about the same or slightly higher. For amplifier B, MPP–, saturation was not seen at 101.000 e^-, or 35000 ADU.

7 Charge Transfer Efficiency

The fraction of electrons that are successfully moved from one pixel to another during read-out is described by the charge transfer efficiency (CTE).

The CTE has been measured using a ^{55}Fe X-ray source, whose emissions generate a specific number of photo-electrons on the CCD for each detection. The read-out counts as a function of position on the CCD can then be converted to a CTE value.

The values found are:

Serial CTE:	0.999999
Parallel CTE:	0.999995

Transporting the charge from the most remote corner of the CCD to the output amplifier will then lead to a 1.2% loss of charge to the following pixel. No difference in performance between using amplifier A and B was found.

Note that CTE strictly speaking is a function of exposure level, so the value given here may not be applicable to all cases. Near zero level and full well, CTE may be poorer than the value found.

8 Modulation Transfer Function

The transparency of Silicon depends strongly on wavelength. At long wavelengths, QE is low due to a high transparency, e.g. at $950nm$ half of the light is absorbed at a depth of $36\mu m$, which is more than the typical thickness of a thinned CCD. At short wavelengths absorption occurs near the surface, e.g. at $400nm$ half of the light is absorbed after $0.15\mu m$.

The potential well of the pixel-defining electrodes does not extend all the way to the surface of the CCD. Photo-electrons generated near the surface may then diffuse to neighbor pixels, causing a degradation of the image sharpness.

In MPP+ mode, the three parallel phases are all "low", while in conventional MPP– mode, one of the phases is "high". The high phase increases the attracive force on the photo-electrons, making the diffusion slightly less significant.

The effect of diffusion can be seen in the Point Spread Function intrinsic to the Silicon, or in it's Fourier transform, the Modulation Transfer Function. A thorough examination of the MTF of a CCD is presented at *http://www.astro.ku.dk/~ijaf/mtf/mtf.html*, while the method is described in [Andersen, M. I. 96]. Below, a few results are given.

The measured MTF is shown in figure 4 for illumination wavelengths of 670nm and 830nm. In the same figure, the expected MTF due to the pixel geometry is shown. A rather poor MTF is clearly demonstrated. Some instrumental effects are not are not removed from the data, but the impact on the result is minor.

The analysis of the MTF data for the W19-(0,0) has not been completed, but the raw data appears very similar to data for another well examined CCD from the same batch, and data for this CCD is therefore presented below.

The MTF is measured in one dimension, for which the spatial equivalent is the Line Spread Function (LSF). From the LSF, a two-dimensional pixel PSF is calculated. The effective pixel size can be defined in several ways. Here we use the Strehl equivalent width, i.e. 1 / SQRT(pixel Strehl ratio), and get:

Wavelength [nm]	**Width [pixels]**
543	2.24
670	1.85
830	1.52

9 Quantum-efficiency

Quantum efficiency vs. wavelength: With backside charging and a HfO_2 coating, the QE reaches it's maximum value of more than 90% from 450nm to 500nm, as can be seen in the QE vs. wavelength plot in figure 5. Shortwards of 400nm, the QE is decreasing, but remains relatively good, with approx. 57% QE at 334nm. Towards long wavelengths, QE decreases steadily due to the increasing transmission of the Silicon of the thinned CCD. For observations in the $1.0\mu m$ to $1.1\mu m$ range, one might try using a CCD temperature of -80°C to increase the sensitivity slightly, but the dark current will increase also and warm columns will appear.

Stability of the sensitivity: In order to achieve high blue sensitivity, the Loral CCDs are thinned and back side illuminated. Still, short wavelength photons are absorbed near the back surface, in a region where the potential from the electrodes is not felt. To drive the photo-electrons towards the front side, charging of the back side by UV-flooding was applied to CCDs previously used on the ALFOSC. The charging proved sensitive to contamination, resulting in unstable QE.

For this CCD, a Steward Observatory "Cat-C" coating is used. The coating creates a potential difference at the Si surface large enough to force the electrons to the front side. In contrast to earlier coatings based on Platinum, this coating has proved to be insensitive to contamination from out-gassing when the liquid Nitrogen is used up.

Several global-scale QE measurements are displayed in figure 5. The QE is determined from the sigma-clipped average ADU count of a 400 by 400 pixel area at the center of the CCD. Some quite small changes in QE can be seen, at max. The cause of this will be examined in the following.

Two curves are indistinguishable, dated December 02 and 04. In between, the CCD was kept at -100°C. This provides the ideal environment for QE stability. The January 30 graph shows slightly better QE over the entire wavelength range. For this measurement, the strongly concave FOSC entrance window was used, while for other measurements, a flat window was used. The difference in QE results from a not quite perfect compensation for the attenuation from the FOSC window. Also, another controller was used, so another gain determination had to be used. For this reason, the difference between December and January data is not considered significant.

The December 02 and January 30 were both made immediately after two days of storage at room temperature in the poor vaccuum from out-gassing after the liquid Nitrogen tank runs dry. This has for other coatings caused decrease of QE, but here it remains unchanged.

The change in local structure can be examined in figure 6 for 1060nm light, figure 7 for 550nm and figure 8 for 334nm With a few exceptions, the local structure is unchanged. At all wavelengths, low-sensitivity specks are seen, the the QE of some of these is not stable. Both increase and decrease of about 10% in relative sensitivity can be found in the central area of a few of these specks.

Some of the dark specks in the short wavelength flat field images are apparently caused by a locally too weak potential from the coating. The potential can be increased in these regions by UV-flooding in an Oxygen atmosphere. An example of the improvement in flat field uniformity is shown in figure 9. Many of the small low-sensitivity specks have disappeared. In figure 5, the December 05 measurement has been made after UV-flooding. The global short wavelength QE appears to have increased by about a percent after flooding. In fact, the QE outside the specks is unchanged - the change in measured QE is only due to the increased QE in the specks.

The stability of the UV flooding while the CCD is cold has not been checked. Previous experience with the lack of stability of UV-floodable CCDs suggests that flooding to remove the specks is not worth the effort. Leaving the camera warm in vacuum for a few days completely removed the effect of UV-flooding: the specks went back to the original low sensitivity.

While the stability of QE is good under normal operation, the sensitivity can be dramatically reduced under other circumstances. After dismounting and re-installing the CCD into the camera, a large area with low sensitivity appears, as shown in figure 10. The sensitivity was seen to drop by as much as 1/3 of the original level at 334nm. The area was developed on two occasions, both showing exactly the same structure, indicating the area is not defined by the distribution of a contaminationg material, but is a property of the coating. Some constituent of atmospheric air must be causing this, possibly water. The QE is gradually re-gained when the CCD is in vaccuum at room temperature, and if the CCD is heated to +50°C for an hour while evacuating the cryostat, the QE is completely restored afterwards. Note that this problem does not occur even if the Nitrogen supply is exhausted. Only direct exposure to atmospheric air has been seen to cause problems.

10 Bias and overscan

The CCD has hardware overscan regions of two columns at each end of the serial register. These areas are somewhat too small for a high signal to noise measurement and are suspected to be affected by the illumination of the imaging area, so they are not recommended as bias level reference.

The recommended type of "extended" overscan can only be used for read-out windows extending to the edge of the CCD opposite of the amplifier being used, as it is generated by continued clocking and read-out after the last image column.

Overscan in the X-direction is set by the "xover" command, and in the Y-direction by "yover". The Y-overscan is of little practical use, though. To get the overscan region in the image, the window size must be specified to go beyond the border of the CCD by the width of the overscan. E.g. An image of the section [1500:2052,something] with a X-overscan width of 50 using the A-amplifier would be defined like this:

ampl A
xover 50
xbeg 1500
xsiz 602 (i.e. $602 = 2052 + 50 - 1500$)

And when using the B-amplifier, an image with overscan must begin at x=1, e.g. for an image with 650 imaging pixels and 50 overscan pixels, the set-up would be:

ampl B
xover 50
xbeg 1
xsiz 700

The default x-overscan size is 50 and zero in the y-direction. Post-processing by BIAS will always make the x-overscan appear at the right border of the image, whatever amplifier is specified.

A comparison between two bias frames is shown in figure 11. The two frames were separated by seven exposures, in all two hours apart. An offset in the level between the two images of about 1 ADU is seen. To minimize this, the temperature of the CCD and electronics should be kept stable. By applying an offset based on the overscan level, the bias drift can be corrected.

A strong gradient is present in the X-direction. As the gradient reproduces well, it should not create problems. Amplifier B was used, making the overscan region appear next to the region with the strong gradient.

In the Y-direction a bias level fluctuation of about 1 ADU amplitude is seen during read-out. The variation is sufficiently slow to make tracking of the variation using the extended overscan possible, making bias subtraction to better than 1 ADU feasible.

11 Dark current

The amount of dark current depends on the CCD temperature and the MPP mode used. Here, only the standard operating temperature of -100°C is considered.

In the default MPP+ mode, dark current is found to be approx. $2e^-$/pixel/hour. Actually, only about half of this is real dark current. The other half is caused by the pressure sensor that emits light quite strongly. A baffle has been put in front of the sensor, reducing the light level to about the dark current level, and distributing the light evenly over the CCD.

In MPP– mode, the dark current is approx. $9e^-$/pixel/hour. As MPP– mode is expected to provide a slightly better MTF, the increased dark current may be acceptable for many applications.

If several long exposure dark images are median filtered and bias subtracted, a completely flat image results. No structure or hot pixels have been found.

A 1800sec, MPP+, Amplifier B, -100 °C dark exposure is shown in figure 12. Except for re-binning, no processing have been made. A horizontal gradient is seen next to the overscan region. The structure is removed by bias subtraction.

12 Pixel size

By illuminating the CCD with collimated light through a grid of pinholes with known separation, the following dimensions were found for a CCD from the same batch as W19-(0,0) :

Pixel size in serial direction: $15.03 \pm 0.02 \mu m$
Pixel size in parallel direction: $14.99 \pm 0.01 \mu m$

This is consistent with the design specifications of $15 \mu m$ square pixels.

13 Cryostat

The cryostat liquid Nitrogen tank is tilted relatively to the CCD to achieve an upright position when mounted on the ALFOSC with the telescope pointing towards Zenith. This is done in order to maximize holding time.

Spilling will occur if the dewar is tilted shortly after filling. Filling in the morning after observations will result in the least spilling during observations. In this way, one filling per day may be sufficient.

Filling the dewar by using a tube connected to a pressurized tank will result in overflow a bit before the tank is full due to gas in the tube. An hour after filling, a tilt of more than 45 degrees can be applied without any liquid Nitrogen spilling out. This means that most observations can be made shortly after filling without a significant reduction in holding time.

Filling by pouring liquid Nitrogen into the dewar using a funnel or lifting the mouth of the pressurized filling tube to flush with the opening of the cryostat allows the tank to become more full before spilling. This can add more than two hours of holding time compared to the pressurized filling method, but requires less tilting of the dewar after filling.

A 90°tilt without spilling requires the tank to be less than half full. The elapsed time after filling, where spilling is avoided has not been determined precisely, but 15 hours after a pressurized refill, no spilling occurred from a 90 degree tilt.

Holding time, with CCD at -100°C: 32 hours till rise of cold finger temperature, and at least one hour more till rise of CCD temperature. If the scoop filling method is used, three hours can be added. The CCD temperature remains at -100°more than 1 hour after the temperature of the cold finger begins to rise. During this period, the pressure rises about a factor of 50. The temperature of the cold finger is about -193°C when there is LN_2 in the tank.

The required time for a room-temperature camera to reach a CCD operating temperature of -100°is approximately 3 hours. The relatively long time is due to a thin cold finger, implying less Nitrogen consumption.

With the CCD temperature control set to a very low temperature, the CCD temperature will not go lower than -115°C. With a full LN_2 tank, the CCD temperature can be forced to about ambient temperature by setting the CCD reference temperature to, say, +30°C. This is again due to the thin cold finger.

Pressure, CCD at -100°C should not be much above 10^{-6} mBar. After the LN_2 is exhausted and the camera returns to room temperature, the pressure will be about 10^{-1} mBar. Evacuation before cooling again is recommended.

The pressure sensor emits light. This has not been detected in previous designs, as the sensor was further away from the CCD. A baffle has been placed in front of the sensor, reducing the illumination. Less than one electron per pixel per hour originating from the sensor is detected on the CCD. The distribution of the light is uniform.

References

[Andersen, M. I. 96] Andersen, Michael I. & Sørensen, Anton N. : **An interferometric method for measurement of the detector MTF**, ESO Workshop on optical detectors for astronomy, in press.

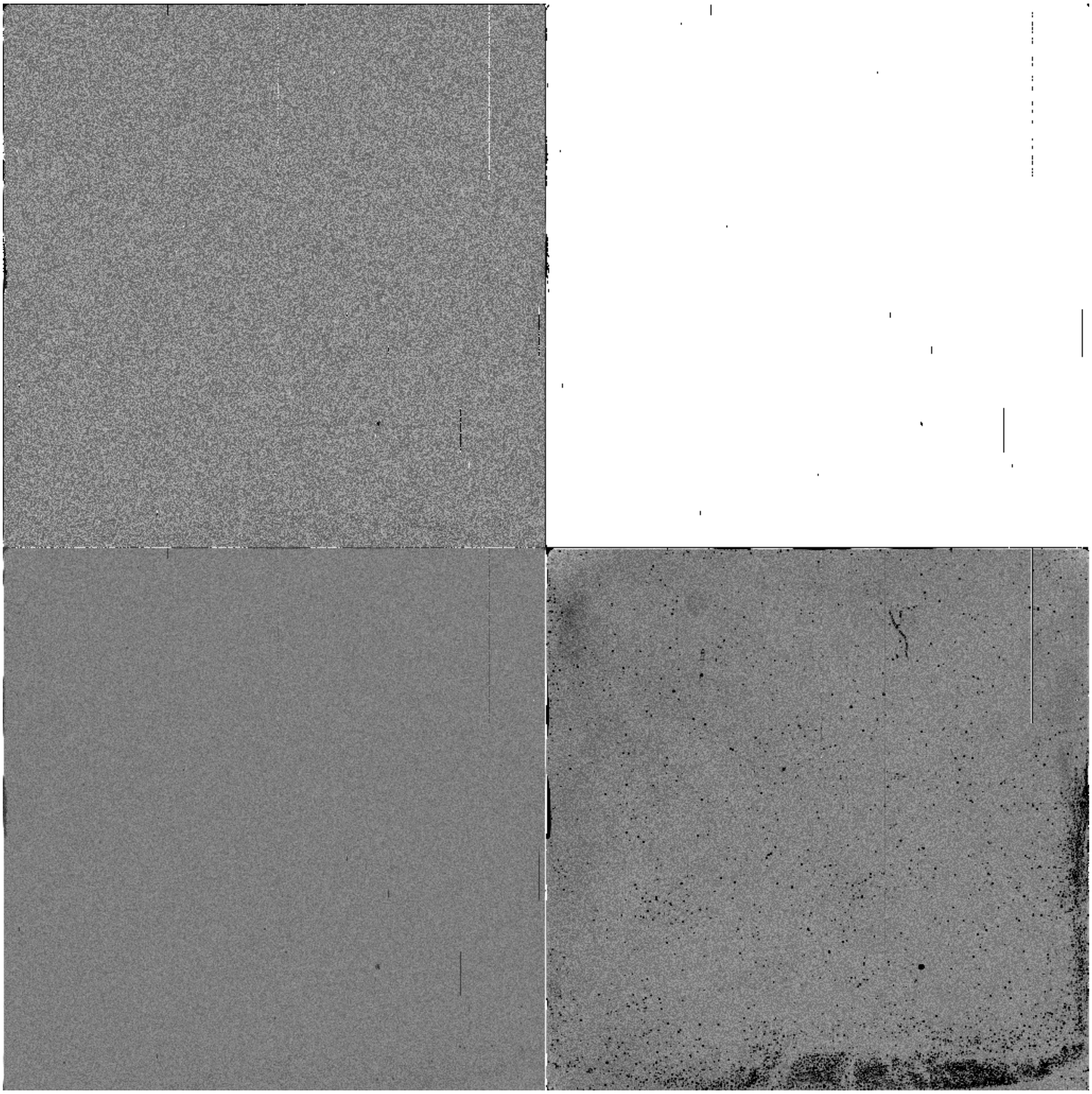

Figure 1: Low illumination level flat field properties, as a mean of identifying charge traps. *Lower left:* Flat field at an illumination level of $71e^{-}$/pixel. Grey scale cuts are $\pm$ 300% of median level. *Lower right:* Flat field at an illumination level of $71.000e^{-}$/pixel. Grey scale cuts are $\pm$ 10% of median level. *Upper left:* Ratio of the two flat fields. Note that nearly all low sensitivity spots are not seen here, indicating that flat-fielding of these is possible and that low-level linearity is good. The vertical lines show areas affected by low level traps. Grey scale cuts are $\pm$ 200% of median level. *Upper right:* Deviating points in the ratio image, affected by traps.

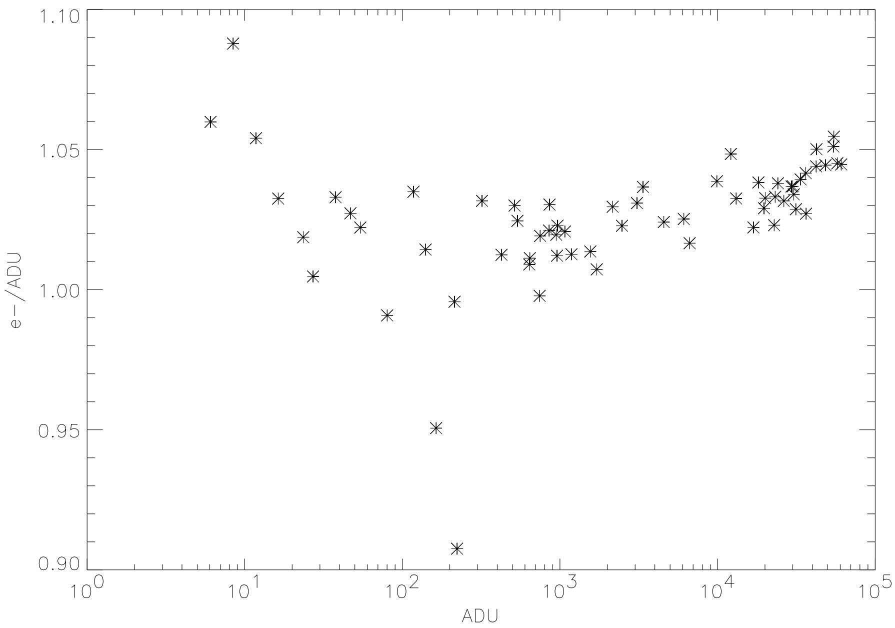

Figure 2: Gain versus exposure level measured from noise statistics for amplifier B in high-gain. The gain apparently changes by 5% over the dynamic range, but change is shown to be much smaller by the more precise measurement plotted in figure 3.

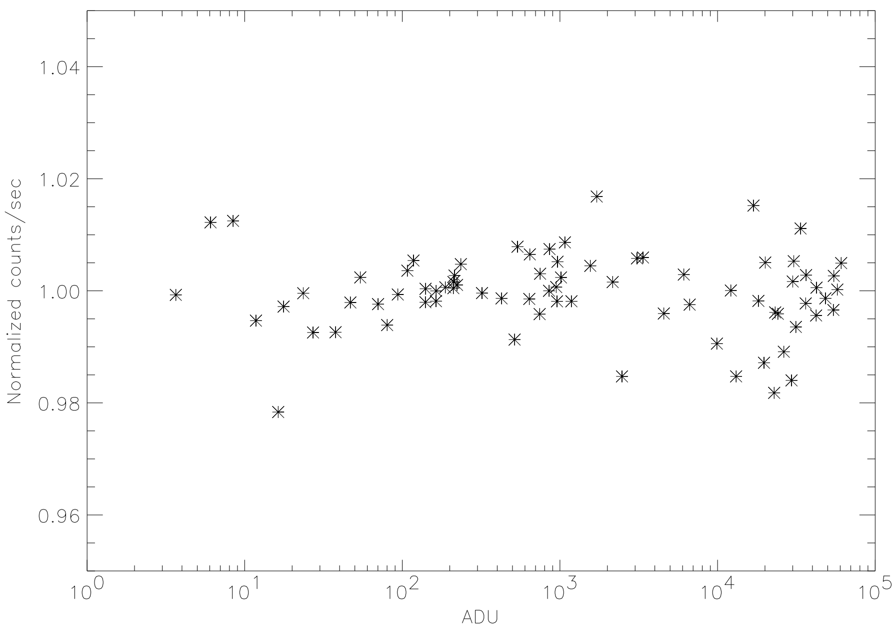

Figure 3: A plot of ADU per second versus total exposure time, corrected for shutter delay. No significant linearity deviation is detected over four decades in exposure range. Amplifier B in high gain was used.

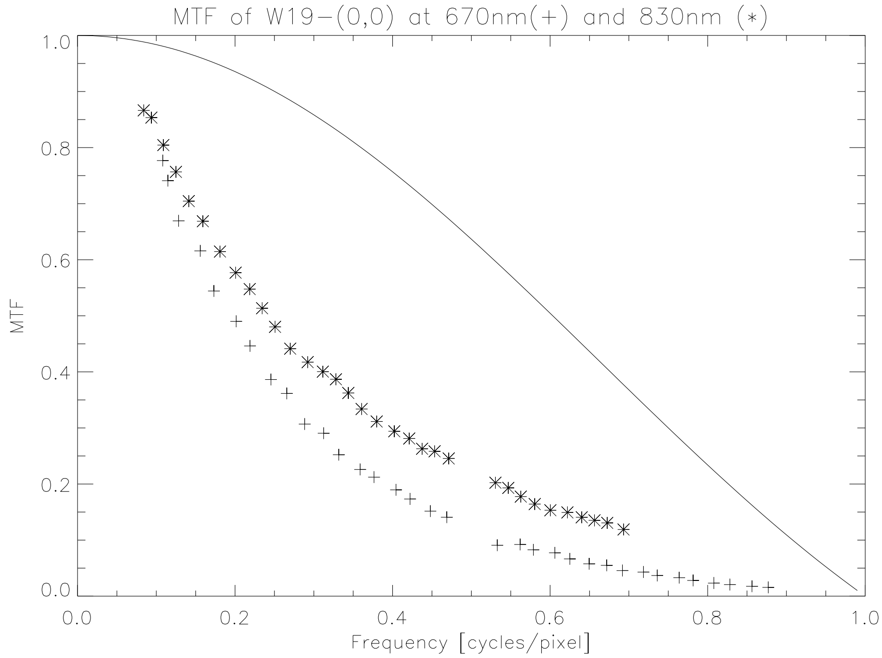

Figure 4: MTF measured for 670nm illumination, shown by plusses, and for 830nm, shown by stars. The fully drawn graph represents the MTF defined by the pixel geometry. The difference between the curves is mainly caused by charge diffusion. The 630nm MTF is worse than the 830nm MTF, as the absorption depth is shorter for shorter wavelengths.

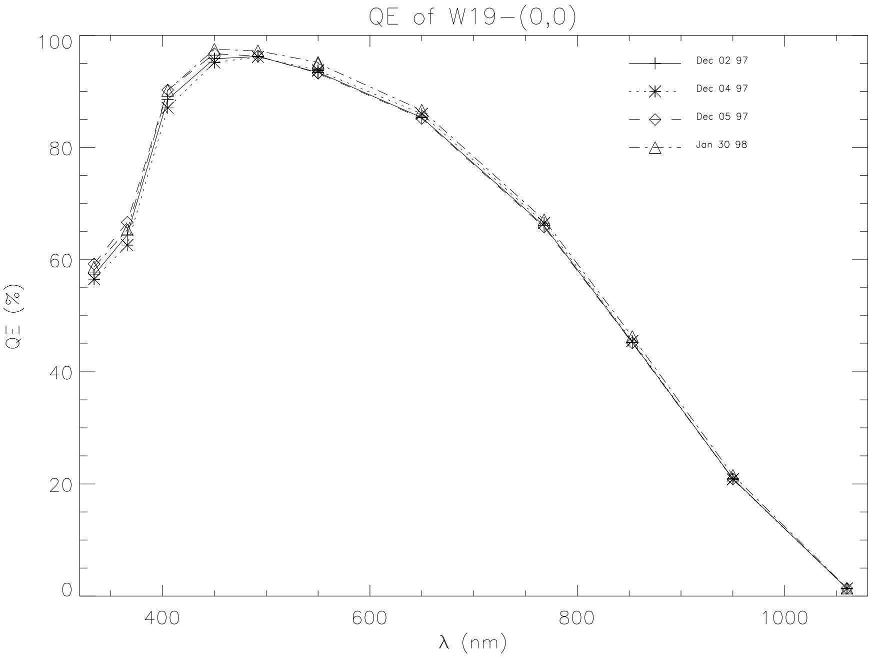

Figure 5: Global quantum efficiency versus wavelength for the W19-(0,0) CCD, measured from the sigma-clipped mean of the central area of a flat field exposure. Although recorded after highly different treatments, from UV-flooding to a few days warm in poor vacuum, the QE is nearly unchanged.

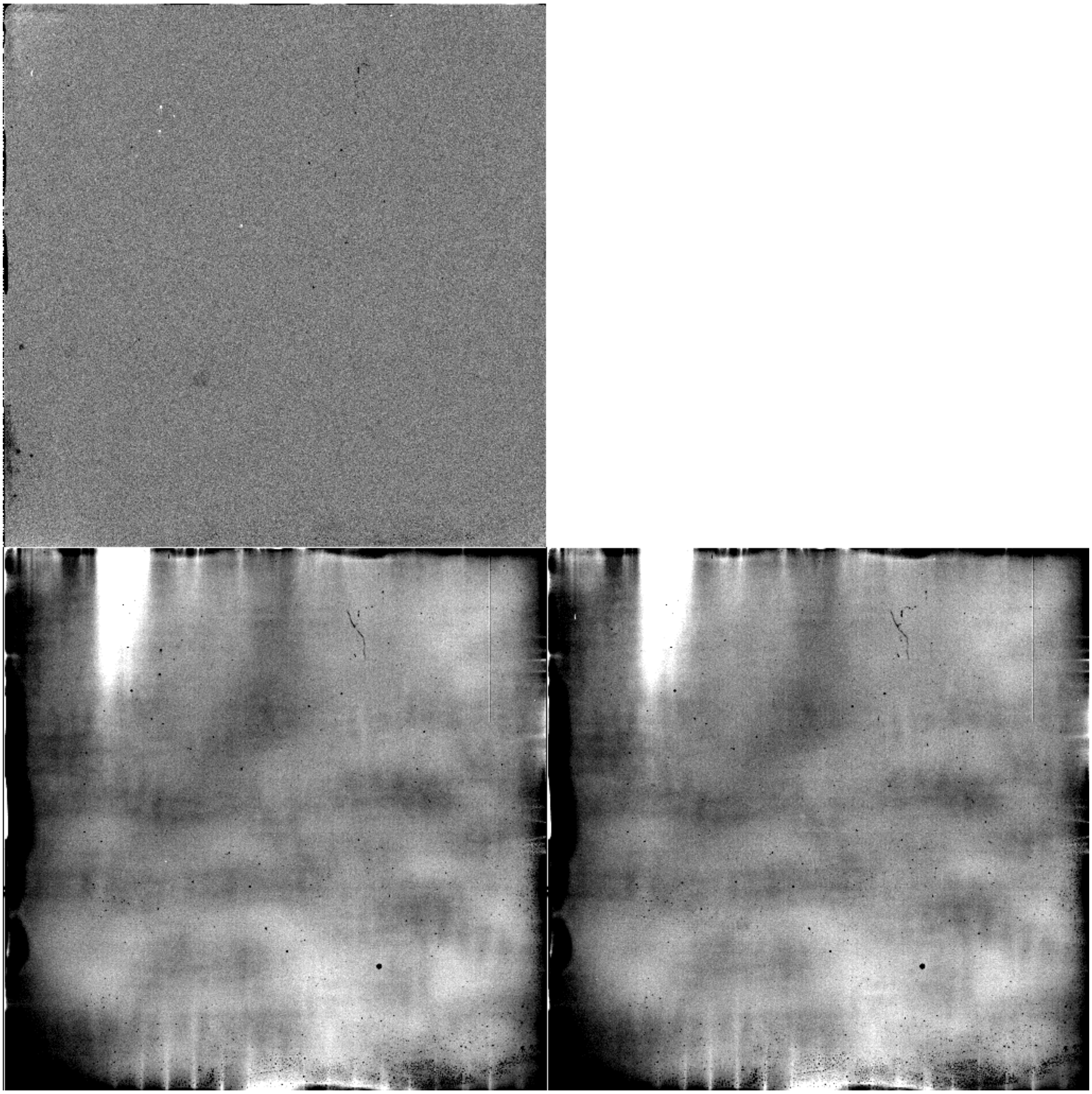

Figure 6: Flat field properties at 1060nm. *Lower left:* The greyscale cuts are set to $\pm 5\%$ of the median level. The large scale structure with a peak to peak amplitude of about 10 % directly relates to the thickness of the CCD, almost completely transparent at this wavelength. The vertical lines at the bottom is light reflected off electrodes below the CCD. The low sensitivity specks are relatively faint. *Lower right:* 28 days later, the structure is essentially unchanged, although the CCD has been UV-flooded, dismounted in atmospheric air, left warm in vacuum and cold-cycled several times. *Upper left:* Ratio between the two flat fields, displayed with cuts of $\pm 4\%$. The large scale flat field structure is unchanged below the detection limit in the central area, but near the edges, some changes of about 1% are seen. In a few specks, the sensitivity has changed by about 3%. During entirely cold periods, QE changes have not been found.

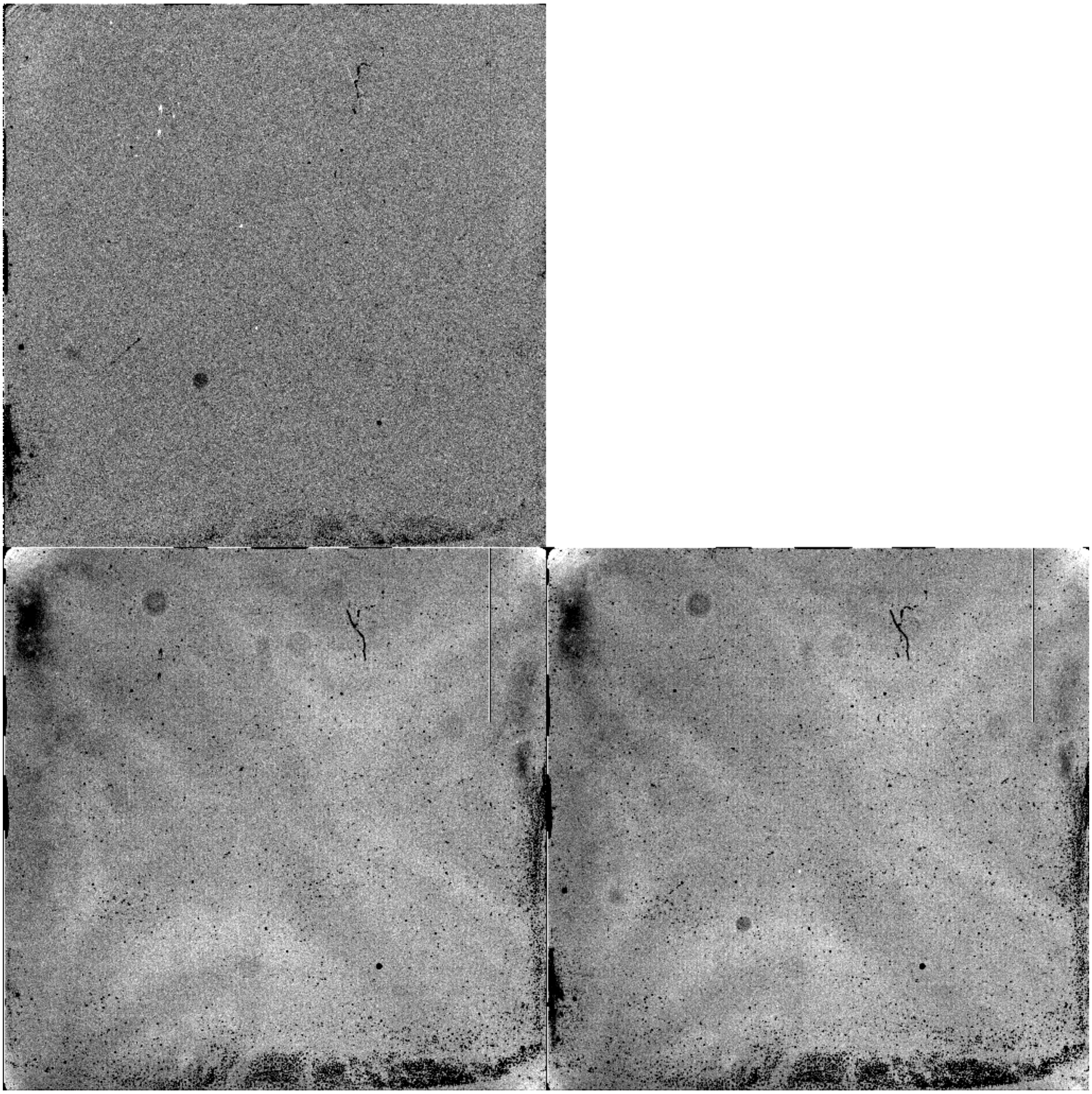

Figure 7: Flat field properties at 550nm. *Lower left:* The greyscale cuts are set to $\pm 2\%$ of the median level. Uniformity is best around this wavelength. Peak to peak large scale structure is about 1%. *Lower right:* 28 days later, the structure is essentially unchanged, although the CCD has been UV-flooded, dismounted in atmospheric air, left warm in vacuum and cold-cycled several times. *Upper left:* Ratio between the two flat fields, displayed with cuts of $\pm 2\%$. Except for a few displaced dust specks, the central large scale flat field is unchanged to within 0.2%, but with 2% changes near the edges. In a few of the low sensitivity specks, the QE has changed by about 10%. During entirely cold periods, QE changes have not been found.

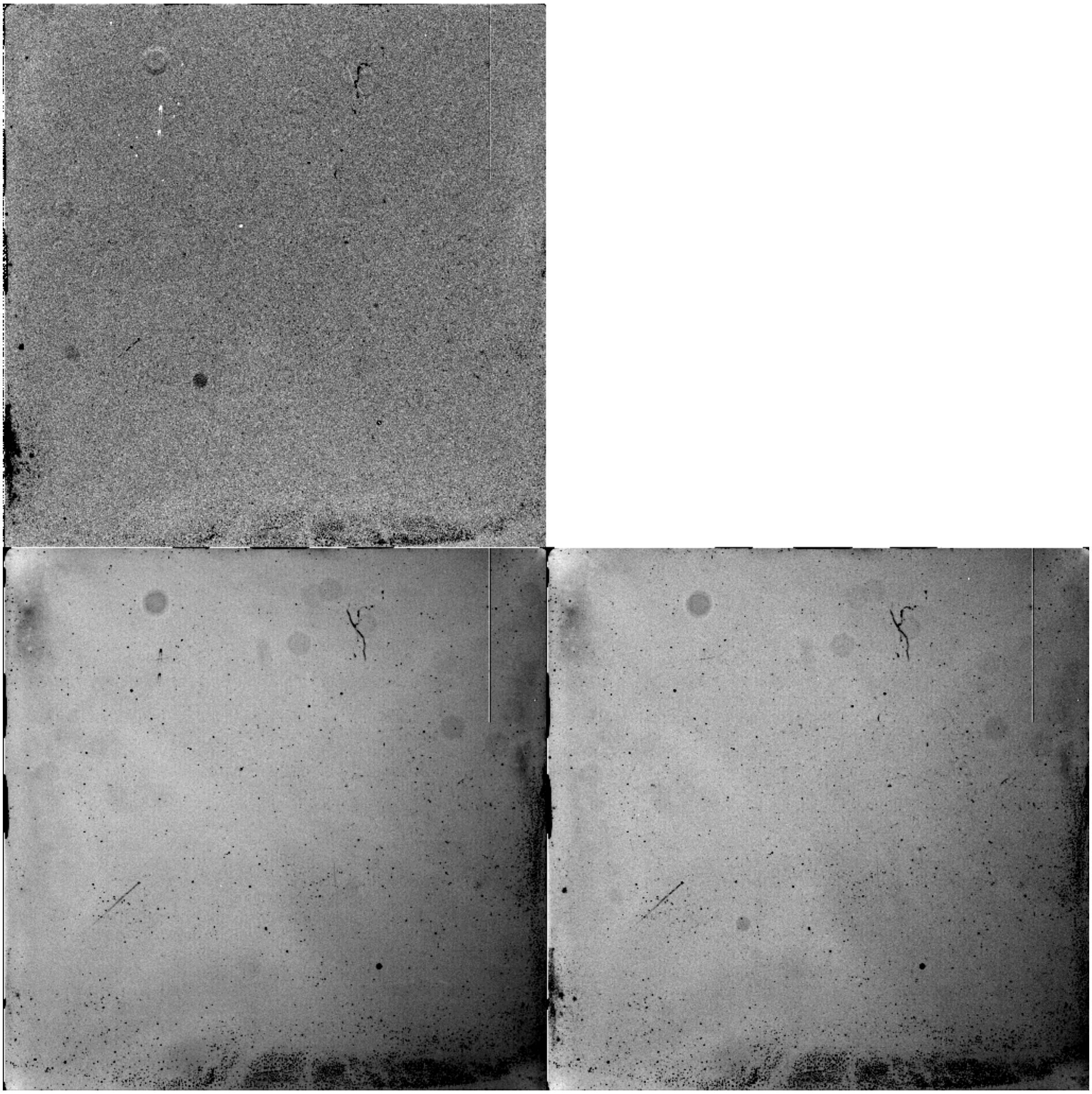

Figure 8: Flat field properties at 334nm. *Lower left:* The greyscale cuts are set to $\pm 5\%$ of the median level. A 5% gradient is seen across the field. *Lower right:* 28 days later, the structure is essentially unchanged, although the CCD has been UV-flooded, dismounted in atmospheric air, left warm in vacuum and cold-cycled several times. *Upper left:* Ratio between the two flat fields, displayed with cuts of $\pm 2\%$. The central large scale flat field is unchanged, but 2% changes are found near the edges. In a few of the low sensitivity specks, the QE has changed by about 10%. During entirely cold periods, QE changes have not been found.

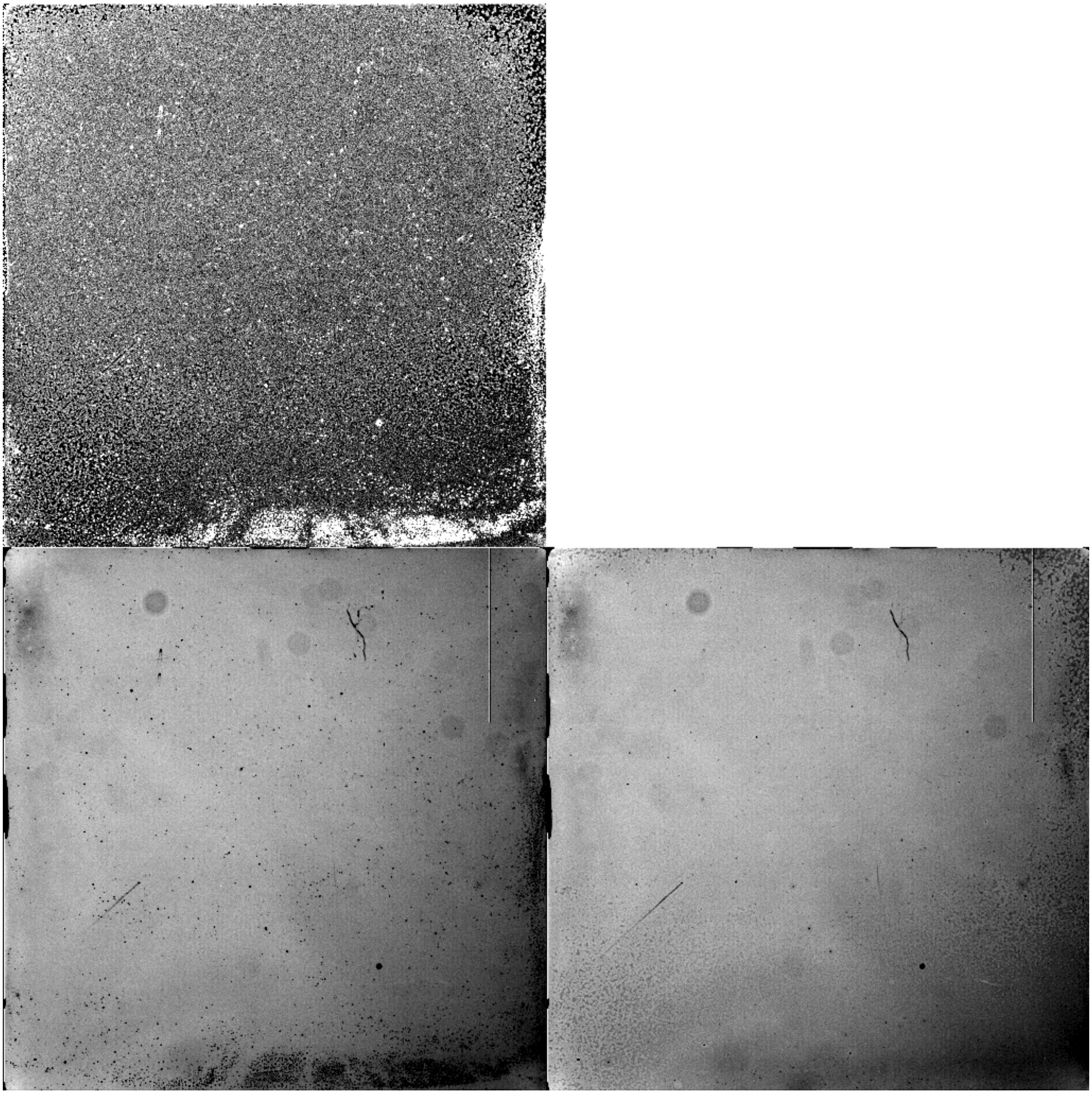

Figure 9: Effect of UV-flooding for 334nm flatfields. *Lower left:* Flat field before flooding. The greyscale cuts are set to ±5% of the median level. *Lower right:* 3 hours after UV-flooding. Most of the low sensitivity specks are gone. *Upper left:* Ratio between the two flat fields, displayed with cuts of ±1%. Areas with increased QE from UV-flooding appear bright.

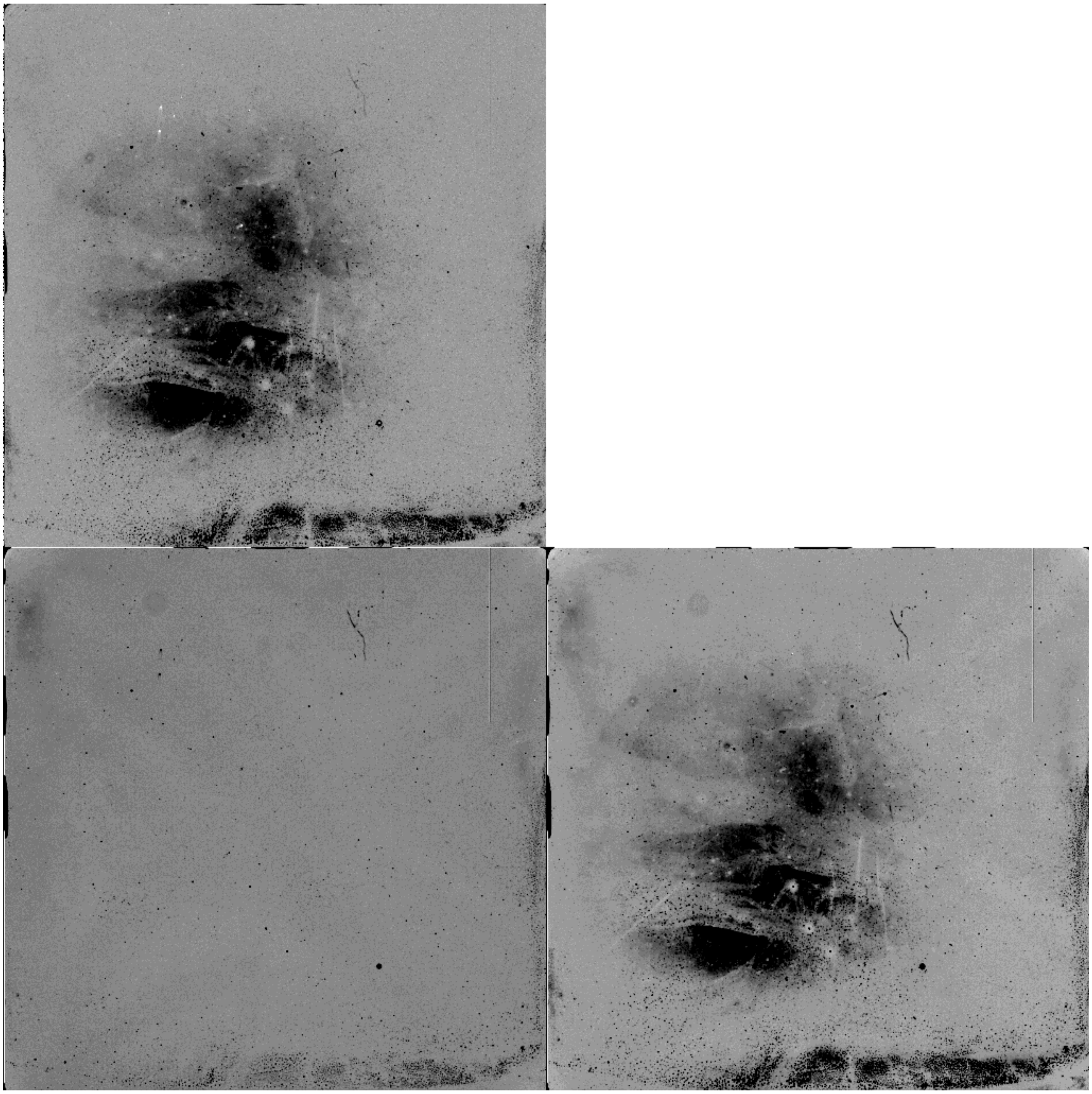

Figure 10: Damage after exposure to atmospheric air: *Lower left:* 550nm normal flat field. *Lower right:* 550nm flat field made after the CCD was stored in atmospheric air for a few days. *Upper left:* Ratio between the two flat fields. In the central region, the relative QE has decreased by up to 35%. All greyscale cuts are set to $\pm 10\%$ of the median level.

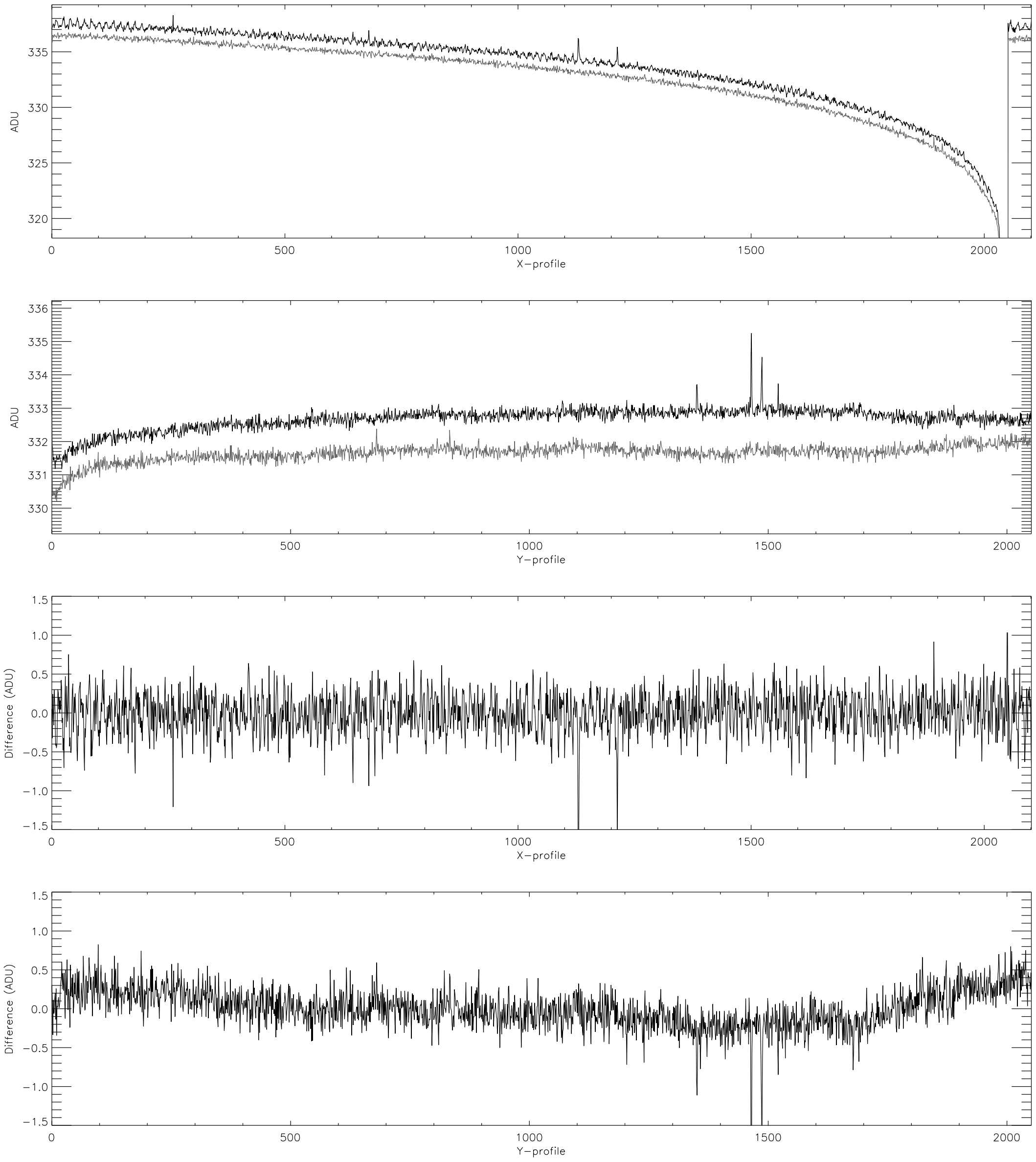

Figure 11: Structure of, and differences between two bias frames, made two hours apart. Amplifier B in high gain, mpp mode was used. In the upper plot, the X-profiles of two bias frames are displayed. A strong gradient is present, and the bias level has drifted about 1 ADU. The "extended" overscan covers columns 2053 to 2102. In the plot below, the Y-profiles are shown, and in the two plots at the bottom, the differences between the profiles are shown with the global drift subtracted. In the X-direction, difference between the images is below detection level, and the overscan tracks the bias level well. In the Y-direction, which is the direction of the parallel shift, a bias level drift during read-out is visible, with an amplitude of approx. 1 ADU. By tracking the overscan level in the Y-direction, this structure can be eliminated. If the read-out window does not extend over the edge of the CCD, the extended overscan will not be available.

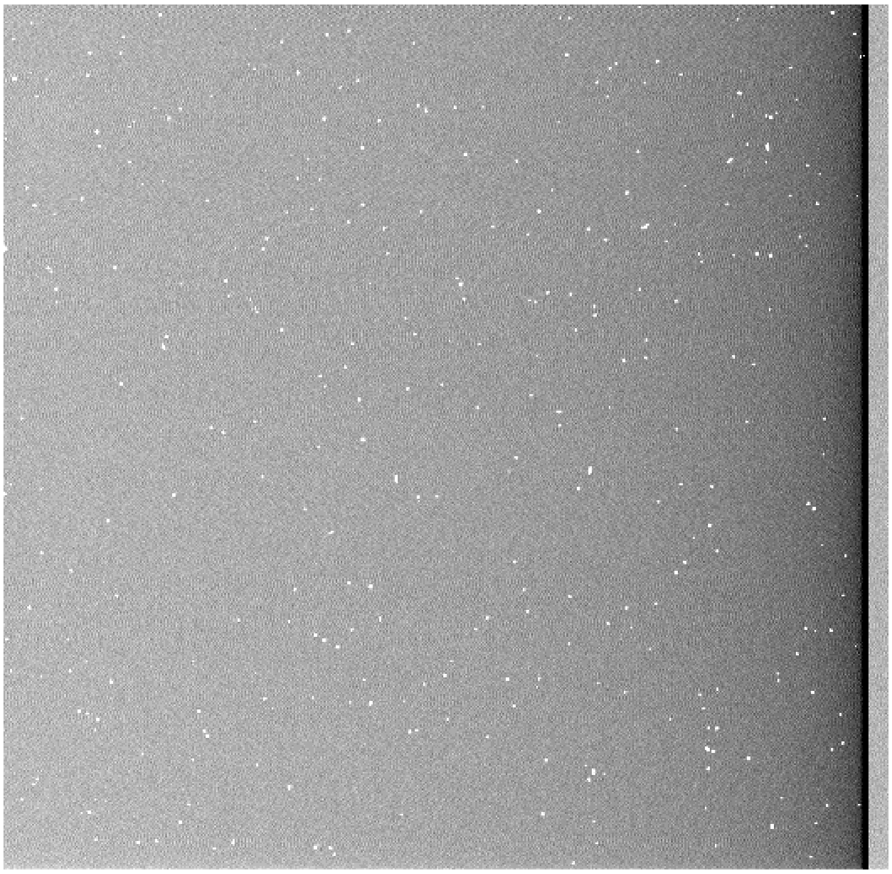

Figure 12: A 1800sec, MPP+, Amplifier B, -100 °C dark exposure. Except for re-binning, no processing have been made. Note the absense of any hot spots or columns. Only cosmic hits are visible, which appear stellar-like due to the poor MTF. The horizontal structure will be corrected by bias subtraction.